

Lawrence Berkeley National Laboratory

Lawrence Berkeley National Laboratory

Title

Interactions of Antiprotons in Hydrogen, Beryllium, and Carbon

Permalink

<https://escholarship.org/uc/item/7hk3d6d7>

Author

Cork, Bruce

Publication Date

1960-03-01

UNIVERSITY OF
CALIFORNIA
Ernest O. Lawrence
Radiation
Laboratory

INTERACTIONS OF ANTIPROTONS
IN HYDROGEN, BERYLLIUM, AND CARBON

TWO-WEEK LOAN COPY

*This is a Library Circulating Copy
which may be borrowed for two weeks.
For a personal retention copy, call
Tech. Info. Division, Ext. 5545*

UCRL-8746

UC-34 Physics and Mathematics
TID-4500 (15th Ed.)

UNIVERSITY OF CALIFORNIA

Lawrence Radiation Laboratory
Berkeley, California

Contract No. W-7405-eng-48

INTERACTIONS OF ANTIPROTONS
IN HYDROGEN, BERYLLIUM, AND CARBON

Bruce Cork

(Thesis)

March 1960

Printed in USA. Price \$1.50. Available from the
Office of Technical Services
U. S. Department of Commerce
Washington 25, D.C.

INTERACTIONS OF ANTIPROTONS
IN HYDROGEN, BERYLLIUM, AND CARBON

Contents

Abstract	3
I. Introduction	5
II. Description of Antiproton Experiment	7
III. Experimental Results, Elastic, Inelastic, and Charge-Exchange Scattering	15
IV. Comparisons with Nucleon-Nucleon Scattering	19
V. Calculations of Pion-Exchange Potential	25
VI. Optical-Model Calculations	28
VII. Applications of the Optical Model	33
A. n-p, p-p, and \bar{p} -p Scattering	33
B. Quantum-Mechanical Modifications	33
C. Calculation of Diffraction-Model Angular Distribution	34
VIII. Scattering of Antiprotons from Beryllium and Carbon	
A. Experimental Results	36
B. Comparison with Calculations	40
C. Polarization Calculations	40
IX. Fermi Statistical Model	43
X. Conclusions and Discussion	44
Acknowledgments	46
Bibliography	47

INTERACTIONS OF ANTIPROTONS
IN HYDROGEN, BERYLLIUM, AND CARBON

Bruce Cork

Lawrence Radiation Laboratory and Department of Physics
University of California, Berkeley, California

March 1960

ABSTRACT

To determine the nature of the interactions between anti-nucleons and nucleons, it has been necessary to do an experiment in which the elastic, inelastic, and charge-exchange interactions could be measured. Improvements in the 6-Bev Bevatron have permitted production of a considerably larger flux of antiprotons, than was available in earlier studies. With the use of strong-focusing magnetic quadrupoles, a crossed electric- and magnetic-field spectrometer, and time-of-flight scintillation counters it has been possible to detect approximately 30 antiprotons per minute. By means of a system of 4π solid-angle scintillation counters, it has been possible to measure these cross sections, including the angular distribution of elastic scattering. These cross sections have been measured for antiprotons scattered from hydrogen, beryllium, and carbon in the energy range from 133 to 333 Mev.

Ball and Chew have assumed that pion exchange is responsible for the nucleon-nucleon interaction, and have used field theory to calculate the antinucleon-nucleon interaction. They have assumed that the pionic charge of the antinucleon is opposite that of the nucleon; thus, the exchange of an odd number of pions should change the sign of the potential. Outside the hard core, the exchange is assumed to be due to two pions, and the sign of the potential is not reversed for either the nucleon or the antinucleon case.

With this model, Ball and Chew have very effectively predicted the absorption and elastic cross sections from 50 to 200 Mev. Ball and Fulco have extended the calculations to 260 Mev and determined the differential and charge-exchange cross sections, again in good agreement with present experiments.

The measured values of antiproton scattering from hydrogen, beryllium, and carbon are well described at small angles by the optical model. The inelastic cross section is approximately one-half the total cross section at these energies. The measured values are shown to be in agreement with certain theories and in disagreement with other theories. Further experiments to more thoroughly test the theories are suggested.

I. INTRODUCTION

Although nucleon-nucleon forces have been most completely described by phenomenological models, there is hope that extensions of quantum field theory will be further developed to more completely and satisfactorily describe strong interactions. The experimental results of measurements of the nucleon-antinucleon scattering, annihilation, and charge-exchange cross sections have stimulated the development of various aspects of quantum field theory. In particular, the work of Ball and Chew¹ has been very successful in predicting the antiproton-proton total, elastic, and charge-exchange cross sections in the energy range from 50 to 200 Mev. They assumed that the hard-core potential calculated for the nucleon-nucleon scattering could be replaced by a "black hole" for the nucleon-antinucleon system. Thus, as soon as the particles approach the critical separation distance, they annihilate. For collisions outside this distance, the nucleons interact through pion exchange, described by a Yukawa pion potential. Then, assuming that the nucleon-nucleon interaction is described by pion exchange, they calculated the nucleon-antinucleon interaction by assuming that the potential changes sign for exchange of an odd number of pions, and does not change sign for exchange of two pions.

By using the Ball and Chew model, Ball and Fulco² have extended the calculations to include scattering, annihilation, and angular-distribution cross sections. The simple model is not expected to be valid for laboratory-system kinetic energies of less than 50 Mev because the WKB approximation is not satisfied for energies that are low compared with the interaction potential. Also, the model is not expected to be valid for energies greater than 260 Mev because of nucleon recoil effects, and penetration of the core by higher partial waves.

The model has been very successful in describing the nucleon-antinucleon interaction, and also in describing the antinucleon-nucleus scattering by means of the optical model.

Koba and Takeda³ have assumed a phenomenological model that divides the region of nucleon-antinucleon interaction into an absorbing core and a surrounding meson cloud. With this model, they are able to account for the high multiplicity of pions and the low multiplicity of K mesons observed in nucleon-antinucleon annihilation.

In this paper the experiment and results of Coombes, Cork, Galbraith, Lambertson, and Wenzel⁴ are briefly described, and results of the extensions of this experiment to measurements of antiproton cross sections in beryllium and carbon are discussed. Comparisons with present theories are made.

II. DESCRIPTION OF ANTIPROTON EXPERIMENT

Because the threshold for producing antinucleons by high-energy protons is approximately 5.4 Bev, kinetic energy, it has been difficult to obtain sufficient antiparticles for scattering experiments. Antiprotons were produced by the 6.2-Bev proton beam of the Bevatron striking a 6-inch-long beryllium target. The yield of antiprotons is shown by Table I. This experiment was designed so that strong-focusing magnetic quadrupole lenses could focus as many antiprotons as possible along a magnetic channel (Fig. 1). To reject some of the background of pions, a parallel-plate velocity spectrometer, with crossed electric and magnetic fields, was used. The antiprotons were then selected according to charge and momentum by deflection in a magnetic field, and identified by time of flight between the six scintillation counters. By this means it was possible to obtain on the order of 30 antiprotons per minute with a background (due to accidental counts of pions) of less than 1%. The channel could be tuned for kinetic energies from 130 Mev to 330 Mev.

Since the annihilation and charge-exchange cross sections, as well as the total and angular-distribution cross sections are very interesting, the apparatus shown in Figs. 2 and 3 was built. The liquid hydrogen target Fig. 4, 12 inches long and 6 inches in diameter, is completely surrounded by scintillation counters as shown in Fig. 5. The counters S and a are cylinders or cones, as indicated, with S_4 and S_5 having a radius about the beam axis of 15 inches. The counters are split into semicylinders or semicones. With this apparatus, the total cross section is measured by determining whether or not an incident antiproton is detected by counter t , and elastic scattering is measured by the number of events in counters S that satisfy the necessary kinematics. The annihilation events are detected by all the counters, including a , while charge-exchange events result in no charged particles detected by the scintillation counters.

Table I

Beam characteristics

The momentum band width is $\pm 5\%$. Yields per proton incident on the beryllium target were measured at the exit of the magnetic channel and correspond to operation with the spectrometer off. Operation of the spectrometer at 300 kv rejects fast particles by the factor shown.

Average momentum (Mev/c) ($\pm 3\%$)	Angle of emergence from target (degrees)	Solid angle (10^{-3} sterad)	\bar{p}/p ($10^{-12} \pm 20\%$)	π^-/p^- ($10^{-6} \pm 40\%$)	\bar{p}/π^- ($10^{-6} \pm 50\%$)	Spectrometer rejection factor ($\pm 20\%$)
600	0	2.2	6	4	1.5	30
700	0	1.8	12	5	2.4	10
800	0	1.6	22	5	4.4	7
900	7	1.4	48	6	8	4

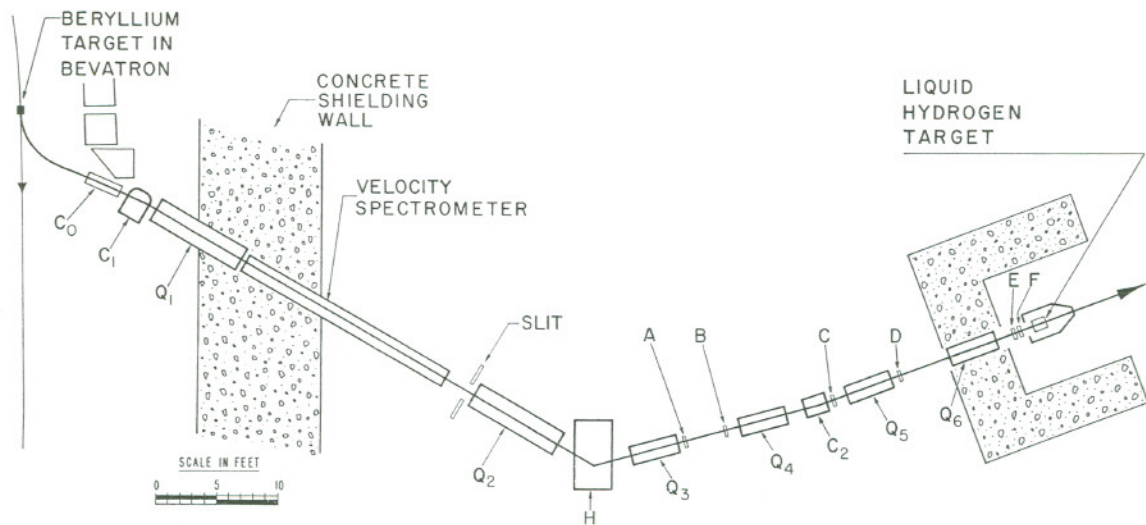


Fig. 1. Experimental arrangement. Compensator C_0 corrects for changes in the Bevatron field. C_1 , C_2 , and H are deflecting magnets. Quadrupole sets Q_1 and Q_2 have 8-inch aperture; Q_3 - Q_6 have 4-inch aperture. Counters A through F are $4 \times 4 \times 1/4$ -inch plastic scintillators used for time-of-flight measurement.

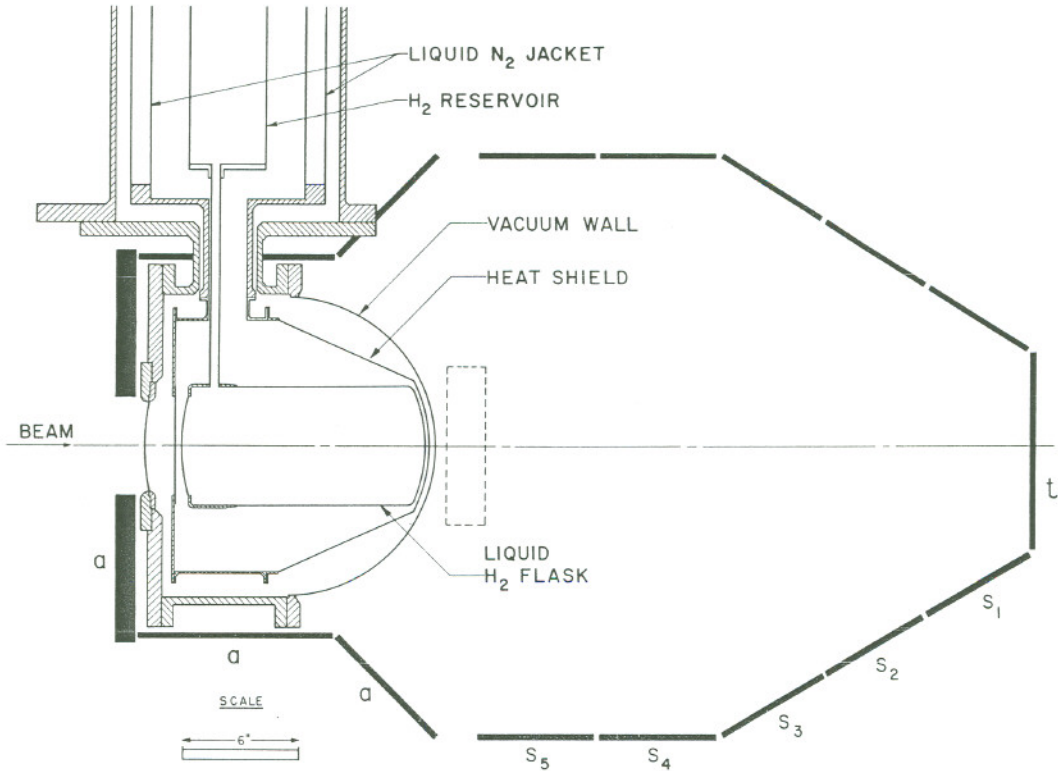


Fig. 2. Liquid hydrogen target and surrounding counters. Target flask of 0.010-inch stainless steel surrounded by a 0.003-inch copper heat shield and a 0.040-inch aluminum vacuum wall in the forward direction (gasket details not shown); a, t, and S₁ through S₅, plastic scintillation counters. The dashed rectangle shows position of a Pb or Al absorber if used to measure annihilation detection efficiency.

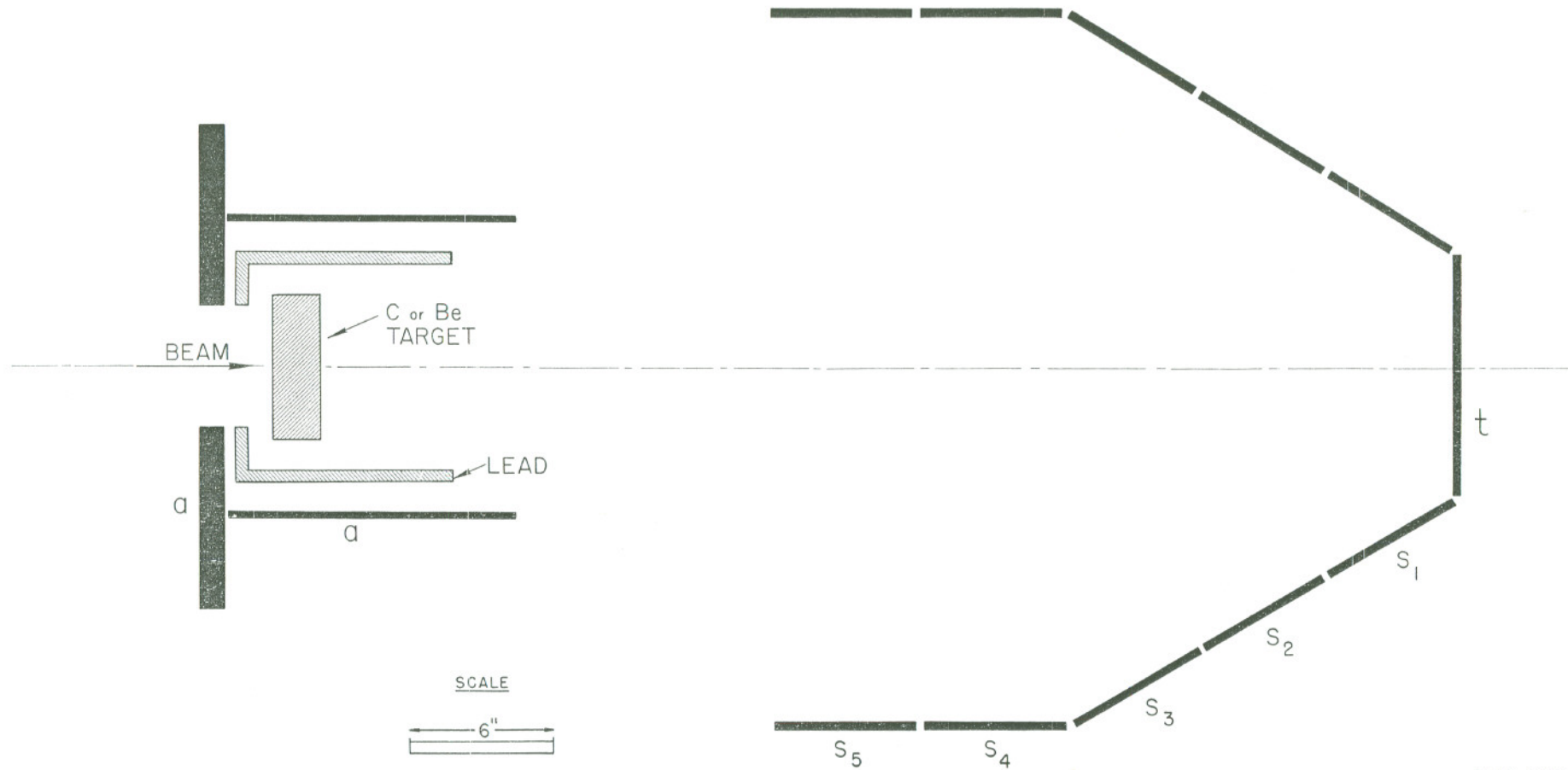
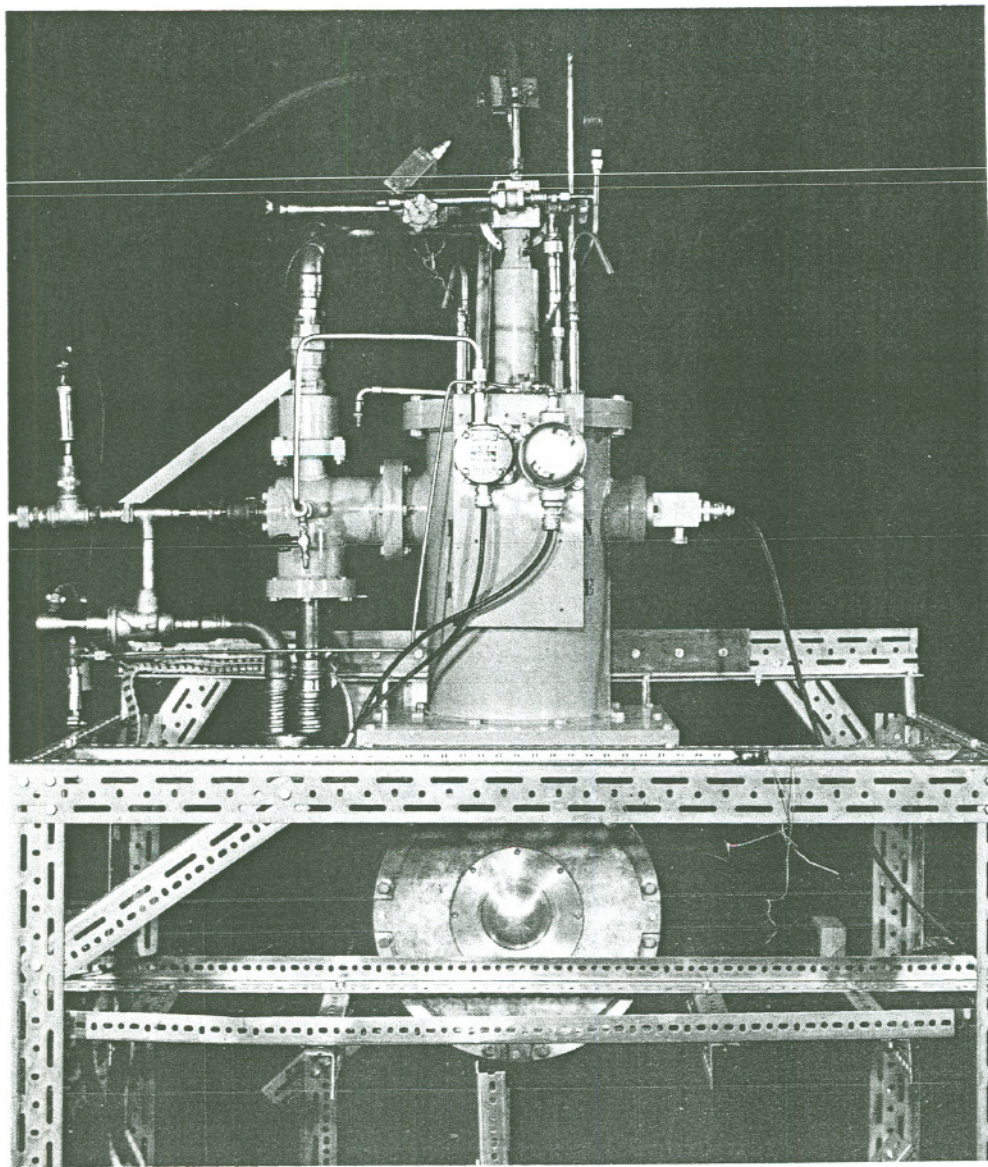


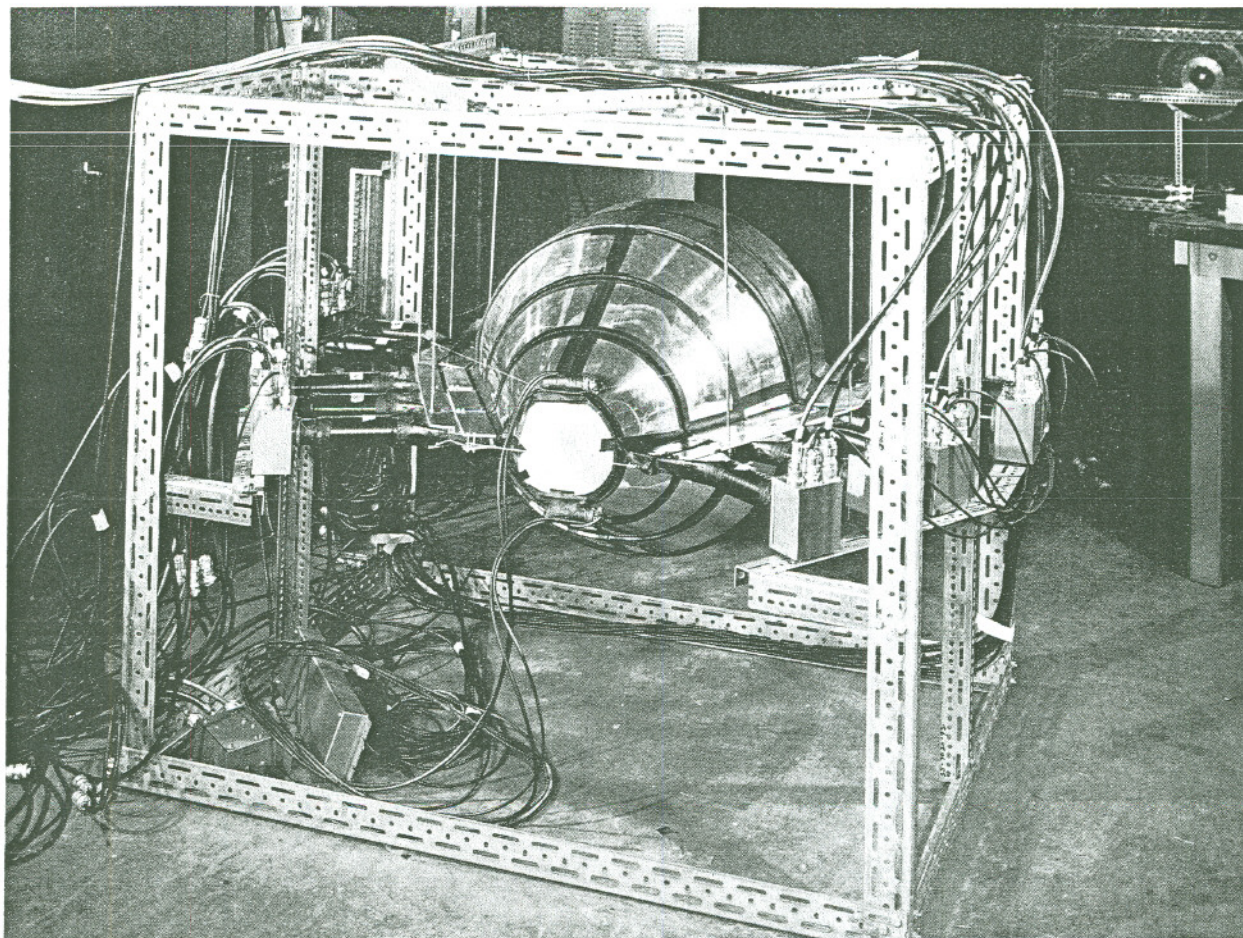
Fig. 3. Carbon and beryllium targets surrounded by scintillation counters.

MUB-389



ZN-2372

Fig. 4. Liquid hydrogen target, viewed from entrance end.



ZN-2371

Fig. 5. Angular distribution scintillation counters. These are split into left and right groups.

The efficiency of the system of counters is very high because most of the light from the terphenyl scintillators is totally internally reflected from the polished surfaces of the scintillators and is detected by photomultipliers. The solid angle for detecting charged particles is nearly 4π steradians, and the γ rays from π^0 mesons are efficiently converted in the Pb that lines the annihilation counters.

For the beryllium and carbon cross-section measurements, the hydrogen target was removed and the α counters were replaced by either 2 in. of beryllium or 2 in. of carbon, surrounded by a 1/2-in. -thick Pb converter and simplified annihilation counters (Fig. 5.)

Further details of the experimental apparatus, magnitude of corrections, and uncertainties are given in a paper already published.⁴

III. EXPERIMENTAL RESULTS: ELASTIC, INELASTIC, AND CHARGE-EXCHANGE SCATTERING

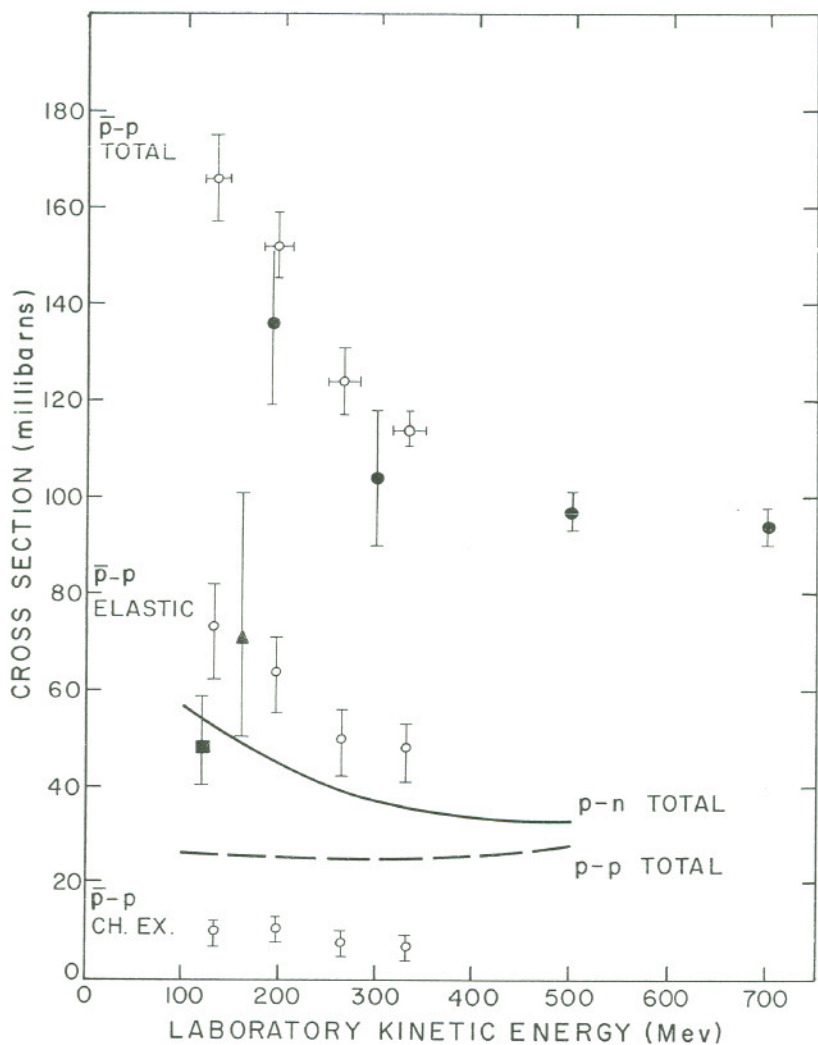
Interactions in the 12-in. -long liquid hydrogen target were detected in coincidence with the antiproton time-of-flight coincidence. Several runs were made at each of four energies, with and without liquid hydrogen in the target. Only 10 to 20% of the antiprotons interacted in the liquid hydrogen and approximately 5% in the target container (metal). The total cross section was measured with a minimum cutoff angle of 14 deg in the center-of-mass system. The angular distribution of the elastic cross section was measured by requiring that only a single s counter counted together with the a counter, or else that only two s counters counted. These were split, left and right. For elastic events, the included angle between the s counters was required to be consistent with the kinematics of an elastic-scattering event in which both scattered and recoil particles were detected.

Inelastic events were detected by counts in counters a , or in more than two s counters. Events in which an incident antiproton did not produce a count in any of the counters was classified as a charge exchange.

The results and corrections are given in Table II and Figs. 6 and 7. The \bar{p} - p elastic, inelastic, and total cross sections show a similar dependence on energy. The total cross sections agree with previous results, and show an inverse velocity dependence over the energy range measured. The inelastic cross section is approximately one-half the total, and the charge-exchange cross section is about 7% of the total. The angular distribution of the elastic scattering is shown in Fig. 8. It is peaked strongly forward, similar to diffraction scattering from a strongly absorbing interaction.

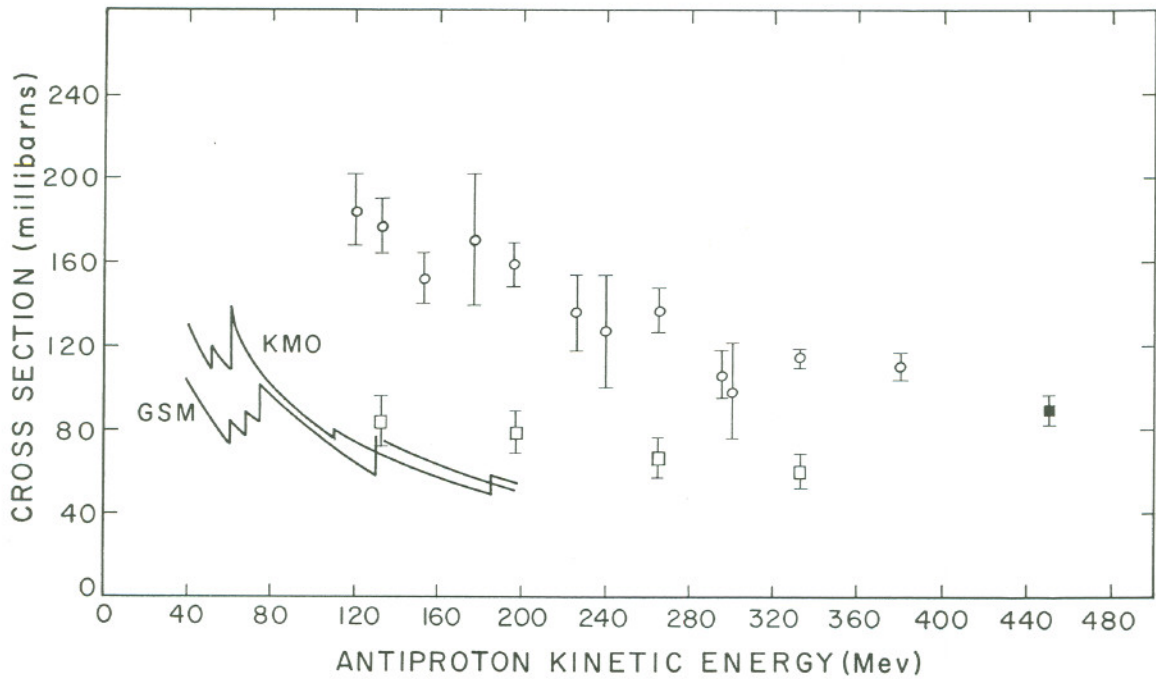
Table II

Antiproton-proton cross sections									
Kinetic energy (Mev)	Total cross section (mb)	Observed elastic cross section (mb)	Minimum cutoff angle (degrees, c. m.)	Maximum cutoff angle (degrees, c. m.)	Forward-scattering correction (mb)	Backward-scattering correction (mb)	Corrected elastic cross section (mb)	Charge-exchange cross section (mb)	Inelastic cross section (mb)
133±13	166±8	59 ⁺⁶ ₋₈	14	93	7	6	72 ⁺⁹ ₋₁₁	10 ⁺² ₋₃	84 ⁺¹⁴ ₋₁₂
197±16	152±7	53 ⁺⁵ ₋₇	14	119	8	3	64 ⁺⁷ ₋₉	11 ⁺² ₋₄	77 ⁺¹² ₋₁₀
265±17	124±7	39 ⁺⁴ ₋₅	14	120	8	3	50 ⁺⁶ ₋₇	8 ⁺² ₋₃	66 ⁺¹⁰ ₋₉
333±17	114±4	38 ⁺³ ₋₄	14	121	8	3	49 ⁺⁵ ₋₇	7 ⁺² ₋₂	58 ⁺⁸ ₋₇



MU-15398

Fig. 6. Energy dependence of total, elastic, and charge-exchange \bar{p} -p cross sections. O = this experiment. ● = total cross sections from Ref. 18; ▲ = σ_{elastic} from Ref. 19; ■ = σ_{elastic} from Ref. 23. (For the last point we have made a 7-mb forward-scattering correction). For reference, p-p and p-n σ_{total} in the same energy range are shown. (Indicated uncertainties discussed in the text.)



MU-15,397

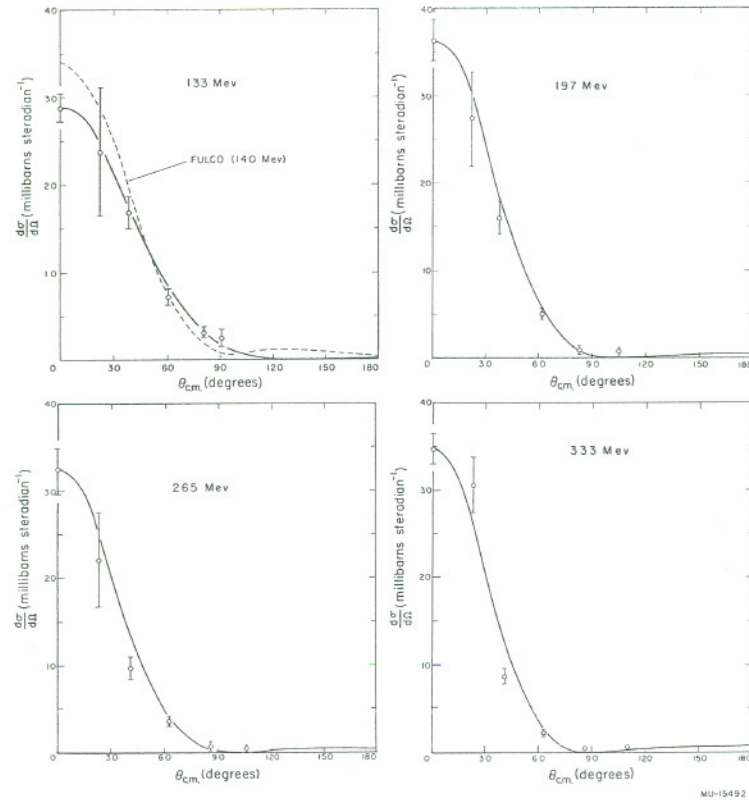
Fig. 7. Energy dependence \bar{p} -p σ_{total} and $\sigma_{\text{inelastic}}$.

For each of the four energies represented in Fig. 6 the σ_{total} data were subdivided into three energies with the help of the chronotron information.

○ = σ_{total} (uncertainties statistical only)

□ = $\sigma_{\text{inelastic}}$ (uncertainties discussed in the text).

The ■ = σ_{annih} (from Ref. 19). The — = theoretical energy dependences of $\sigma_{\text{inelastic}}$ for two potentials that give correct p-p and p-n σ in this energy range.



MU-15492

Fig. 8. Angular distributions of the elastic scattering at four energies. Point at $\theta = 0$ obtained from measured σ_{total} with help "optical theorem"-- a minimum value, as predicted for a purely absorptive interaction. The ——— obtained with help of optical model for classical "black sphere" interaction (indicated uncertainties statistical only) - - - - from Ref. 2

IV. COMPARISON WITH NUCLEON-NUCLEON SCATTERING

Quantum mechanics shows that at high energies, it is possible to obtain, from scattering experiments, direct information on the potential that acts between the particles. Thus, the Born approximation is an assumption that the interaction is described by quantum mechanics and that the energy of the interaction is small compared with the particle energy. For high-energy nucleon-nucleon interactions, this would appear to be a reasonable assumption, and the Born formula, for the scattering amplitude, is

$$f(\theta) = \frac{\mu}{2\pi\hbar^2} \int V(r) \exp^{i(\vec{k}-\vec{k}^1) \cdot \vec{r}} d\vec{r}^3,$$

where μ is the effective mass, $V(r)$ is the interaction potential at the radius r , \vec{k} and \vec{k}^1 are the particle wave vectors before and after scattering, and θ is the scattering angle.

The scattering cross section is⁵

$$\frac{d\sigma}{d\Omega} = |f(\theta)|^2$$

and the momentum transfer g is given by

$$g^2 = (\vec{k} - \vec{k}^1)^2 = 4k^2 \sin^2 \frac{\theta}{2}.$$

The scattering amplitude is then related to the potential by the above relation. The angular distribution of scattering is also defined for a given potential. This simple description of the interaction potential has been found quite inadequate to explain elastic proton-proton scattering. At 31 Mev, a tensor force is required to explain the scattering.⁶ In the energy range from 150 to 350 Mev, the elastic cross section is nearly independent of energy and angle, except for small angles at which the Coulomb potential is significant. However, at higher energies the cross section shows a pronounced angular

dependence. For example, at 657 Mev the scattering is quite anisotropic,⁷ and in the region from 1 Bev to 6 Bev the scattering can be approximately described⁸ by an optical model, with absorption. The angular distributions at several energies are shown by Fig. 9.⁹ Proton-proton scattering polarization experiments in the 100-to-350-Mev region have helped to define the possible phase shifts.¹⁰ The threshold for pion production by protons on protons is 290 Mev. Thus, inelastic processes change the angular distributions so that diffraction scattering is expected.

The n-p process is complicated because exchange scattering is observed. Thus the charge, a pion, is exchanged between the incoming neutron and the proton as a result of a scattering collision. If (as assumed) the masses are equal for the neutron and proton and relativistic effects are neglected, the angular distribution in exchange scattering is the same as the distribution of recoil particles in ordinary scattering. However, the differential cross section distribution about 90 deg in the c. m. system need not be symmetric because the scattering at 180 deg depends on the relative magnitude of ordinary and exchange scattering. The differential cross sections for n-p scattering at several energies are shown in Fig. 10.⁹

If an isotopic spin projection of $+1/2$ is assigned to the proton and antineutron, and $-1/2$ to the neutron and antiproton, then a system of two protons can have a total isotopic spin of only unity, $T = 1$. However, the n-p system and the \bar{p} -p system can have both $T = 0$ and $T = 1$. Thus, correcting for the Coulomb and annihilation interaction, one expects the states with $T = 1$ to be similar. A difficulty in the analysis is that the $T = 0$ and $T = 1$ states interfere with each other and the effects of the annihilation interaction are unknown. If the interference term could be neglected, or subtracted, the scattering cross section for the $T = 0$ state could be determined for the non-annihilation interactions. In some cases, it should be possible to do this by assuming isotopic spin invariance,¹¹ and since the total number of neutrons plus protons scattered at an angle θ is

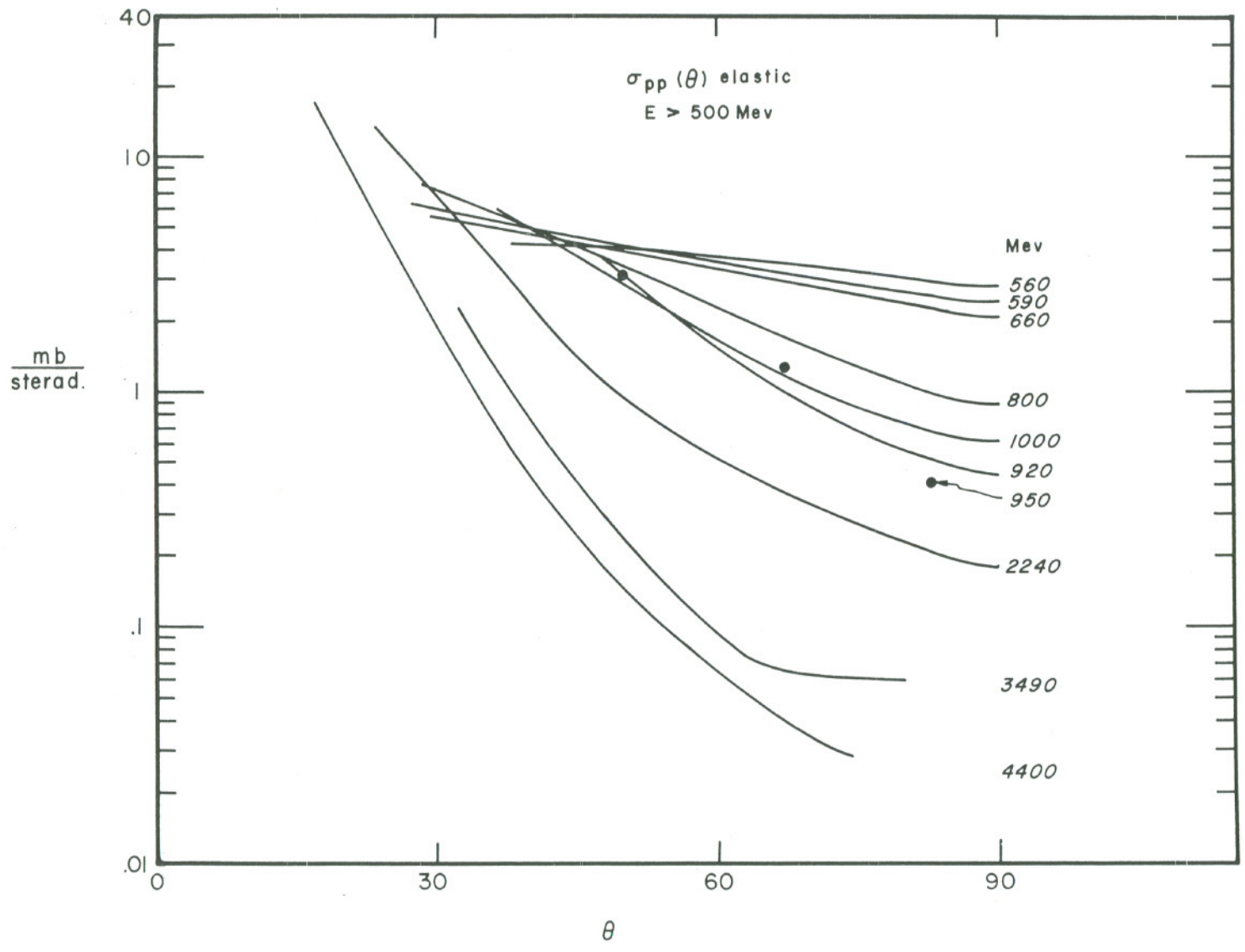


Fig. 9. Experimental values for p-p σ_{diff} at various energies above 500 Mev.

$$\sigma_{np}(\theta) + \sigma_{np}(\pi - \theta),$$

then the sum of the $T = 0$ and $T = 1$ cross sections is

$$\sigma_0(\theta) + \sigma_1(\theta) = [\sigma_{np}(\theta) + \sigma_{np}(\pi - \theta)].$$

Since the p-p cross section is a pure $T = 1$ state, $\sigma_0(\theta)$ can be calculated from the n-p elastic scattering cross sections by subtraction of $\sigma_{pp}(\theta)$.

The differential cross section $\sigma_0(\theta)$ derived in this manner is of course symmetric about $\theta = 90$ deg, and is the average of the forward and backward scattering with the $T = 1$ state scattering subtracted. For the n-p and p-p systems, $\sigma_0(\theta)$ and $\sigma_1(\theta)$ are given by Fig. 11 for 400 Mev.

The nucleon-nucleon isotopic spin systems are:

p-p, n-n, $\bar{p}\bar{p}$, $\bar{n}\bar{n}$, n- \bar{p} , and \bar{n} -p

with $T = 1$, $T_z = \pm 1$,

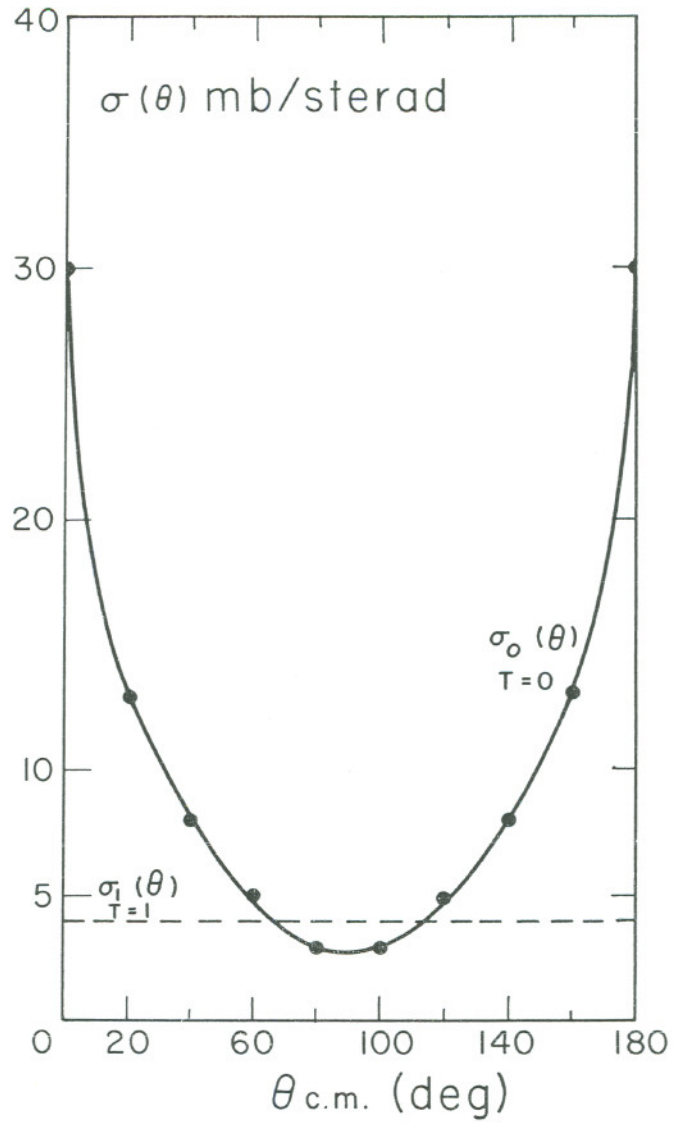
and the mixed states,

n-p, p- \bar{p} , n- \bar{n} , and \bar{n} - \bar{p} with

$T = 1$, $T_z = 0$ or $T = 0$, $T_z = 0$.

In contrast to the p-p and n-p systems, the corresponding antinucleon-antinucleon systems $\bar{p}\bar{p}$ and $\bar{n}\bar{n}$ are very difficult to explore experimentally.

However, the \bar{p} -p system, although not an isotopic-spin doublet system, has $T = 0$ and $T = 1$, and the \bar{n} -p system has $T = 1$ only. Thus, the results of measurements of the \bar{n} -p elastic and annihilation cross sections would be very interesting. Since charge conjugation as well as isotopic spin must be considered, it is difficult to ascertain more about the antinucleon-antinucleon system from antinucleon-nucleon scattering. The hope then is to determine more about the limitations of the statistical model and attempt to find out more about the size of the strong interacting core.



MU-19682

Fig. 11. Angular distribution of n-p scattering at 400 Mev. The $T = 0$ and $T = 1$ states are separated by averaging the θ and $\pi - \theta$ cross sections (see text).

V. CALCULATIONS OF PION-EXCHANGE POTENTIAL

To calculate antinucleon-nucleon cross sections, Ball and Chew¹ have assumed that a particular semiphenomenological model is applicable in the energy range of 50 Mev to 200 Mev kinetic energy. They have assumed a Yukawa type of potential that correctly describes the nucleon-nucleon interaction in this region of energy. Annihilation is described by a short-range absorbing core, and WKB approximation is used to estimate the probability of absorption of each partial wave, and to calculate the phase shifts. Both annihilation and scattering cross sections are obtained in this manner. The repulsive core required to describe nucleon-nucleon scattering is found to have a radius of approximately 1/3 of a pion Compton wavelength.¹² For the nucleon-antinucleon system, Ball and Chew assumed an annihilating core of similar dimensions. In the region outside the core, the one pion-exchange potential was assumed to change sign for the nucleon-antinucleon system. Then, on the assumption of a Christian-Hart effective potential¹³ that includes the spin-orbit interaction, a potential of the general type $V = V_C + \vec{L} \cdot \vec{S} V_{LS} + S_{12} V_T$ is used to construct separate potentials for each eigenstate. The triplet spin-state potential is V_T , V_C is the central force potential, and V_{LS} is the spin-orbit potential. Phase shifts and penetration coefficients are then calculated for the reflected wave, assuming a Gartenhaus potential¹² with a spin-orbit term added by Signell and Marshak¹⁴ that is attractive for short ranges.

With these detailed calculations, Ball and Chew¹ were able to show that because of a cancellation of the effect of the repulsive core against an attractive outside region, the nucleon-nucleon force is small in the region of a few hundred Mev. However, in the nucleon-antinucleon system with an annihilating core this cancellation does not take place. The large cross sections for antinucleons in this energy range are thus explained. The rigorous application of the model predicts "structure" in the energy dependence of the total absorption

cross sections, due to the interaction of succeeding higher orbital-momentum partial waves as the energy is increased. Figure 7 is a plot of the $p\text{-}\bar{p}$ absorption cross section for the energy range of 50 to 200 Mev.

The calculations have been extended by Ball and Fulco to cover the range from 50 Mev to 260 Mev.² They have also used the phase shift calculated for this model to determine the angular distributions for $\bar{p}\text{-}p$ and $\bar{p}\text{-}n$ elastic scattering. Table III is a summary of the results of the calculations by Ball and Fulco² and of the measurements by Coombes, Cork, Galbraith, Lambertson, and Wenzel.⁴ The agreement is observed to be very good except for the absorption cross section at 260 Mev and the charge-exchange cross section. Ball and Fulco have also modified their calculations at 260 Mev to include the effect of partial transmission of the barrier (core). When a transmission of $T = 0.5$ for the triplet D and F waves is assumed, the cross sections are: total, 123; elastic, 58; absorption, 50; and charge-exchange, 15 millibarns, in better agreement with experiment.

Table III

Calculated values^a and measured values^b (in parentheses), of cross sections (in mb) for nucleon-antinucleon interactions at different energies

	50 Mev		140 Mev		260 Mev	
	\bar{p} -p	\bar{p} -n	\bar{p} -p	\bar{p} -n	\bar{p} -p	\bar{p} -n
σ_{total}	232	184	(166)	148	(124)	101
σ_{elastic}	91	93	(72)	79	(50)	64
$\sigma_{\text{absorption}}$	110	91	(84)	69	(66)	37
$\sigma_{\text{charge exchange}}$	31		(10)	21	(8)	15

^afrom Fulco and Ball, Ref. 2

^bfrom Coombes et al., Ref. 4.

VI. OPTICAL-MODEL CALCULATIONS

The optical model used by Fernbach, Serber, and Taylor¹⁵ and modified by Riesenfeld and Watson¹⁶ has been used by Fulco and by Ball and Fulco to calculate angular distributions.² They defined the optical potential

$$V_{\text{opt}}(K) = - [V_{\text{CR}} + i V_{\text{CI}}] \rho(x) + [V_{\text{SR}} + i V_{\text{SI}}] \frac{1}{x} \frac{\delta \rho}{\delta x} (\vec{\sigma} \cdot \vec{l}),$$

where V_{CR} and V_{CI} are the real and imaginary parts of the central potential, and V_{SR} and V_{SI} are the real and imaginary parts of the spin-orbit interaction. The differential cross sections for \bar{p} -p and \bar{p} -n elastic scattering have been calculated for 50, 140, and 260 Mev; Figs. 12 a, b, c show the calculated and measured \bar{p} -p values.

The optical-model potential used by Ball and Fulco can be simplified by assuming that the spin-orbit term is zero. Then the relations between elastic and absorption cross sections can be determined, and the connection with diffraction scattering can be shown.¹¹ The Schrödinger equation for a nucleon of mass m is

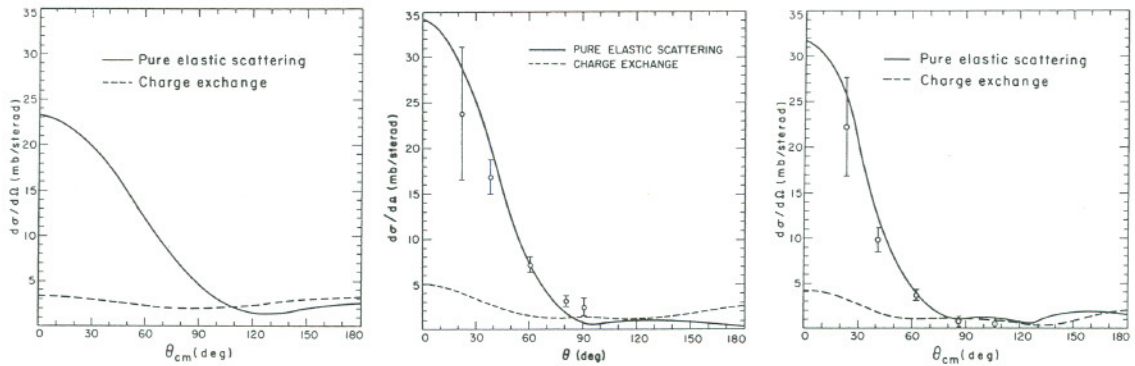
$$E\psi = - \frac{\hbar^2}{2m} \nabla^2 \psi + (U + iV)\psi,$$

where U and V are the magnitudes of the real and imaginary parts of the complex potential. The imaginary potential is associated with the absorption process. To determine the absorption of particles per unit time per unit volume, this equation can be solved in the following manner. First, write the conjugate Schrödinger equation, multiply the first equation by ψ^* , and the second by ψ . The difference of these two equations is, after a bit of rearranging,

$$- \frac{\hbar^2}{2m} \text{div} (\psi^* \text{grad} \psi - \psi \text{grad} \psi^*) - 2V\psi\psi^* = 0.$$

Thus, the real potential U has been subtracted and, since $\psi\psi^*$ is the density of particles, ρ , a current density j can be assigned to the first term, giving the continuity equation,

$$\text{div} \vec{j} = - 2 \rho V.$$



MU-19691

Fig. 12. Differential cross sections in the c.m. system for \bar{p} -p (neglecting Coulomb scattering) and \bar{n} -n interactions at (a) 50 Mev kinetic energy, (b) 140 Mev, (c) 260 Mev, — = pure elastic scattering, - - - = charge-exchange scattering.

The absorption of particles per unit volume per unit time is then just equal to $2V \psi\psi^*$. With the use of this simplified model,¹¹ the potentials U and V can be determined for each energy of the incident nucleon on a nucleon or a nucleus by means of scattering experiments.

The transformed Schrödinger equation is analogous to the general wave equation

$$\nabla^2 \psi + k^2 \psi = 0 ,$$

where $k = (2mE)^{1/2} / \hbar$ is the wave vector for a vacuum. Inside the nucleus this wave vector is a complex number,

$$K = K_1 + i K_2 = \sqrt{(2m/\hbar^2)(E-U-iV)}$$

with a corresponding complex index of refraction,

$$n = (K_1 + i K_2)/K .$$

Inside the interacting nucleus, a particular solution of the wave equation is, for the one-dimensional case,

$$\psi = \exp(i K X) = \exp(i K_1 X) \exp(-K_2 X) .$$

The absorption is then given by the wave vector K_2 associated with the imaginary part of the index of refraction. The diffraction of a nucleon from a nucleon or a nucleus of given radius and optical properties is related to the complex wave vector. Measurements of the differential elastic cross sections and the inelastic cross sections are necessary in order to determine the real and imaginary parts of the potential, and the radius of the nucleus.

For simplified models, the wave equation can be solved both inside and outside the nucleus. At high energies, the wave length of the incident nucleon is small compared with the diameter of the nucleus. Assume a nucleon, described by a plane wave e^{ikz} incident along the z axis and scattered from a spherical nucleus. The magnitude of the wave vector is k in a vacuum and K inside the nucleus.

Assume, as an approximation, that the wave function is a constant except for the shadow region behind the scattering nucleus. Define the phase equal to zero for points in the shadow plane lying outside the shadow region.

Then, outside the shadow region, the wave function is $\psi = e^{ikz}$. The wave function in the shadow region is retarded in phase by an amount equal to the product of the index of refraction and the "thickness" S of the nucleus. Then

$$\begin{aligned}\psi_{\text{shadow}} &= \exp[i (K_1 + i K_2 - k) S] \\ &= \exp[i (K_1 - k) S e^{-K_2 S}].\end{aligned}$$

The nucleon density is, after the interaction,

$$\begin{aligned}\psi\psi^* &= \exp(-2K_2S) \text{ in the shadow region,} \\ &= 1 \text{ outside the shadow region.}\end{aligned}$$

For no absorption, $K_2 = 0$ and the density is unity both in the shadow region and outside the shadow region. Absorption by the nucleus causes the beam to be attenuated to an amount $1 - \psi\psi^* = 1 - \exp(-2K_2S)$, and the absorption cross section is obtained by integrating the attenuation function over the area of the interacting nucleus.

It can also be shown that the elastic cross section for an incident plane wave along the z axis is

$$\sigma_{\text{elastic}} = \int |\psi - 1|^2 dx dy,$$

where, again, the contributions come only over the area of the shadow.

The total cross section is

$$\begin{aligned}\sigma_{\text{total}} &= \int (1 - |\psi|^2 + |\psi - 1|^2) dx dy \\ &= 2 \int (1 - \text{Re } \psi) dx dy,\end{aligned}$$

or, substituting the value of ψ in the shadow,

$$\sigma_{\text{total}} = 2 \int (1 - e^{-2K_2S} \cos (K_1 - k) S) dx dy.$$

Thus, measurements of the differential, elastic, and absorption cross sections will permit calculations of the complex index of refraction and the combined radius of the nucleus plus incident nucleon.

The absorption cross section for a completely opaque nucleus is πr^2 , where r is the radius of the shadow. For high-energy incident nucleons, the wave length is small and the nuclear refraction is large, giving

$$(K_1 - k) S \gg 1 .$$

The second term in the integral for the total cross section,

$$\text{Re } \psi = \exp (-K_2 S) \cos (K_1 - k) S,$$

thus changes sign many times, with the result that the integral of this term over the shadow is small. The total cross section for a black sphere then approaches $\sigma_{\text{total}} = 2\pi r^2$. With this simple model, then, for large absorption,

$$\sigma_{\text{abs}} = \sigma_{\text{elastic}} = \pi r^2 .$$

However, if the absorption is small, then $\sigma_{\text{elastic}} = \sigma_{\text{total}} = 2\pi r^2$. A lower limit of $2\pi r^2$ is then placed on the elastic cross section by this model.

VII. APPLICATIONS OF THE OPTICAL MODEL

A. n-p, p-p, and \bar{p} -p Scattering

This optical model, with modifications, has been used quite effectively to describe the scattering of high-energy neutrons and protons from nuclei. Also, for energies above the threshold for producing pions, the optical model has been used to describe the angular distribution for elastic proton-proton scattering at 1 Bev.¹⁷ Modifications that include a partially transparent nucleon with tapered absorption have been made⁸ to fit fairly well the elastic proton-proton angular distribution from 1 Bev to 6 Bev.

Serious difficulties arose, however, in attempts to apply this simple model to antinucleon scattering. The total antiproton-proton cross section at 500 Mev was observed by Cork, Lambertson, Piccioni, and Wenzel to be 97 ± 4 millibarns.¹⁸ The absorption cross section of antiprotons on hydrogen was observed by Chamberlain, Keller, Mermod, Segrè, Steiner, and Ypsilantis to be 89 ± 7 mb at 457 Mev, nearly equal to the total cross section.¹⁸ Koba and Takeda³ attempted to explain the large absorption cross section in the 500-Mev range in the following manner.

B. Quantum-Mechanical Modifications

The simple classical optical model described above is modified to take into account the quantum character of the high-energy anti-nucleon collision. The tails of the partial waves with high angular momenta can penetrate the centrifugal potential barrier and be absorbed. The effective nucleon radius for absorption is thus increased to $r + \chi$ and the cross section to $\sigma_{\text{abs}} = \pi (r + \chi)^2$. Taking into account the partial waves for $l > 0$, one has

$$\sigma_{\text{abs}}(l) = \pi \chi^2 (2l + 1) (1 - |a|^2)$$

and

$$\sigma_{\text{scat}}(l) = \pi \chi^2 (2l + 1) (|1 - a|^2),$$

where a is defined as the ratio of the amplitude of the outgoing transmitted wave to the incoming wave. To obtain an absorption cross section that is large compared with the scattering cross section, the following inequality must be satisfied:

$$\sigma_{\text{total}} \leq 4\pi \chi^2 (2\ell + 1) [\sigma_{\text{scat}}^{(\ell)}] .$$

Using this relation and a value of 0.2 for the elasticity, Koba and Takeda have calculated that waves at least up to $\ell = 4$ are required to explain the large absorption cross section at 450 Mev.³

Although this difficulty has not been resolved at 450 Mev, the measurements at lower energies, (Fig. 6) show that the elastic and absorption cross sections are nearly equal.⁴ The agreement with the calculations of Ball and Chew¹ is then very good over the energy range from 133 to 200 Mev. Also, the extensions of this theory to 260 Mev, and the calculations of the angular distributions for elastic scattering,² are in good agreement with the experiments (Fig. 12).⁴

C. Calculation of Diffraction-Model Angular Distribution

The angular distributions of the elastic scattering of anti-protons from hydrogen can also be described quite well by assuming a classical "black sphere" interaction. The differential cross section is then

$$\frac{d\sigma}{d\Omega} = k^2 r^4 \left[\frac{J_1 \left(2kr \sin \frac{\theta}{2} \right)}{2kr \sin \frac{\theta}{2}} \right]^2 ,$$

where the effective radius r is determined from the total cross section by

$$\sigma_t = 2\pi r^2 .$$

The solid curves of Fig. 8 show that this simple optical model is a good fit to the data, and probably almost any model that predicts the measured annihilation and elastic-scattering cross sections should

give a similar distribution. The forward scattering calculated by Fulco,² shown by the dotted curve in Fig. 8, is about 10% greater than the minimum given by the "optical theorem" for a purely absorptive interaction. The large-angle scattering is also greater according to Fulco's potential model. The experiments are very difficult for large-angle scattering, so that the preferred model cannot be determined with the present experimental results.

VIII. SCATTERING OF ANTIPROTONS FROM BERYLLIUM AND CARBON

A. Experimental Results

The apparatus that was used for the hydrogen cross-section measurements⁴ was modified, Fig. 3 by replacing the hydrogen target and the annihilation counters by a 2-in. -long beryllium or 2-in. -long carbon target. The targets were surrounded by a 1/2-in. -thick Pb box, so that γ -rays from decay of the π_0 meson would be converted to electrons. The simplified annihilation counters then detected the charged particles from the annihilations. These counters also detected antiprotons that were scattered at laboratory angles greater than 50 deg.

Because of the large number of charged particles produced by the annihilation, these events were generally readily recognizable. Elastic-scattering events were those that gave a count in only one "s" counter. Charge-exchange events did not produce a count in any counter.

Measurements were made for antiprotons of 320 Mev kinetic energy. The forward-scattering correction was made by use of the "optical theorem," which gives the minimum value of the forward scattering. From Figs. 13 and 14 this minimum value appears to be a reasonable correction. The results are given in Table IV and Figs. 13 and 14. The results are in agreement with previous measurements of the total cross sections.¹⁸ The inelastic cross section is somewhat larger than the elastic cross section for both Be and C.

The solid curves in Figs. 13 and 14 are plots of calculations made by Bjorklund and Fernbach of the antiprotons from Be and C.²¹ They assumed the phase shifts calculated by Ball and Fulco for antiprotons-nucleon scattering, and an optical model. Rutherford scattering is shown by the dashed curve.

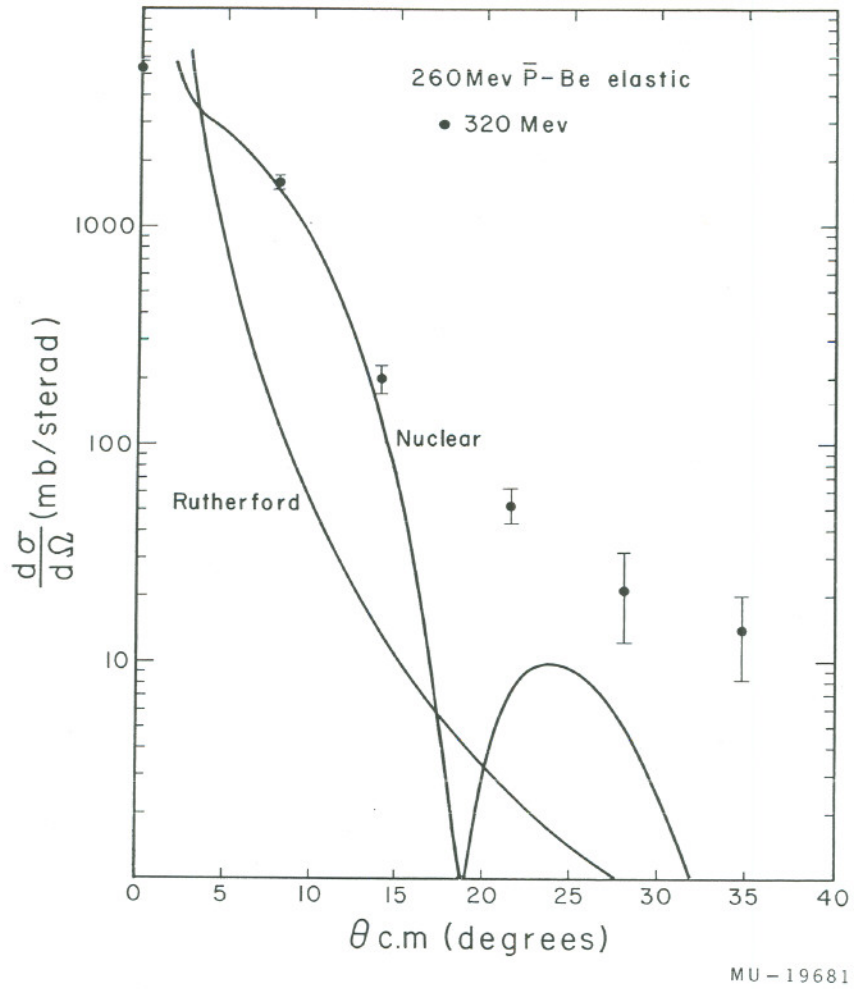
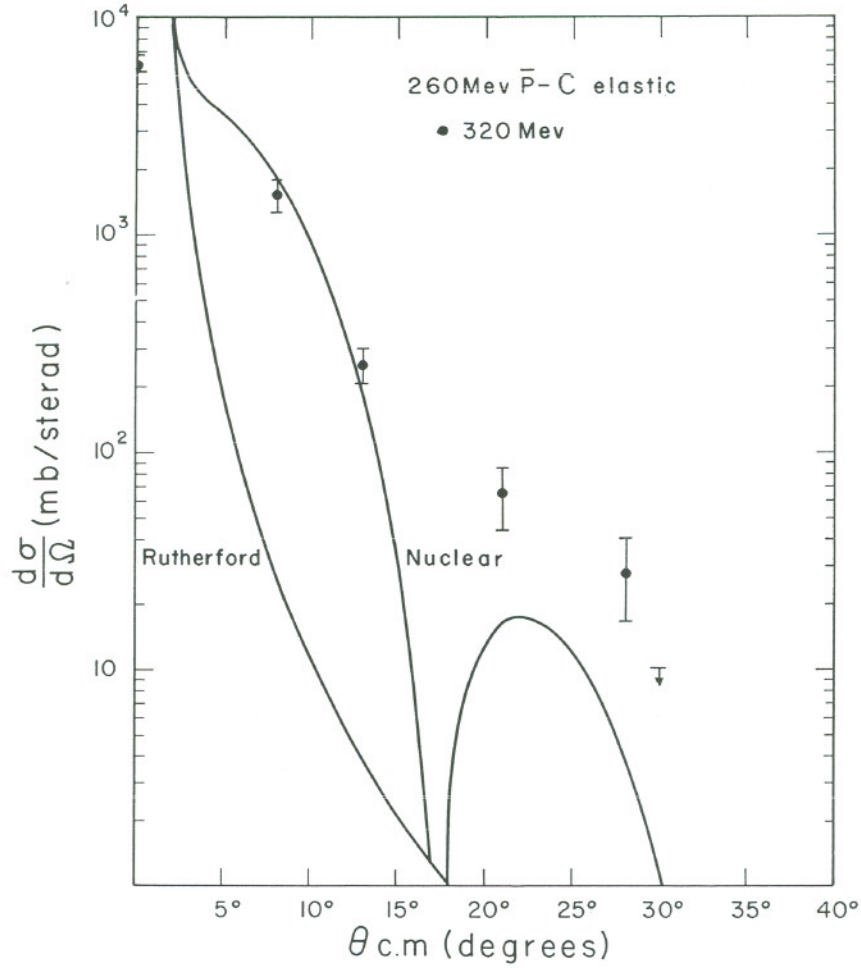


Fig. 13. 260-MeV \bar{p} -Be angular distribution calculations using the optical model, and 320-MeV scattering measurements.



MU-19680

Fig. 14. 260-MeV \bar{p} -C angular distribution calculations using the optical model, and 320-MeV scattering measurements.

Table IV

Total and elastic cross-section measurements at 320-Mev anti-
protons on Be and C

	Measured total cross section	Scattering cross section (5 to 38 deg) (mb)	Forward- scattering correction (mb)	Elastic- cross section (0 to 38 deg) (mb)	Charge- exchange cross section (mb)
Beryllium	670±30	170±10	100±20	270±23	11 ⁺⁴ ₋₅
Carbon	730±40	172±22	125±25	297±40	10 ⁺⁶ ₋₇

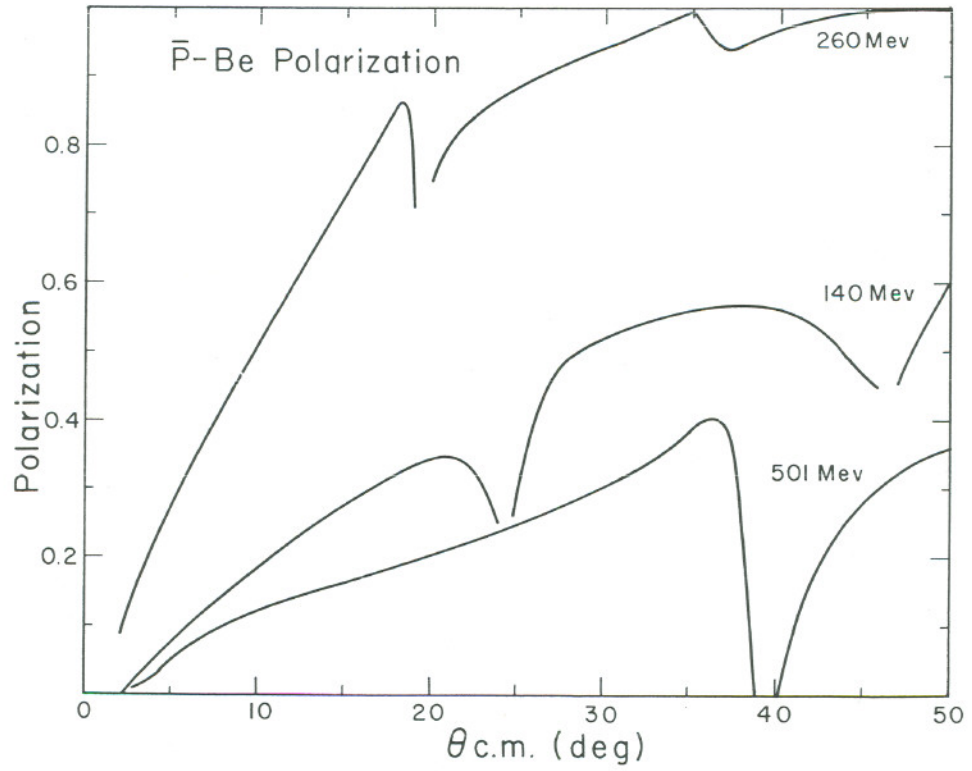
B. Comparison with Calculations

The measured cross sections, at a slightly higher energy, are shown on the same plots. There is good agreement with the calculated values for small angles. The first diffraction minimum may well exist, but the angular resolution of the detection apparatus was not sufficiently small to detect such a minimum.

An optical-model potential calculation has been made by Glassgold²⁰ to fit the reaction cross sections of 140-Mev antiprotons from Ag, Br, and N. He observes that a small value of real potential describes the total cross section, and the very deep potential well postulated by Duerr and Teller²⁰ is not compatible with the experimental results.

C. Polarization Calculations

Calculations of the polarization of antiprotons scattered from Be and C have also been made by Bjorklund and plotted by Agnew,²¹ assuming the Ball and Fulco phase shifts.² These results are shown by Figs. 15 and 16. At 260 Mev, the polarization is very large for both Be and C, i. e., 50% at 10 deg in either Be or C. Antiprotons produced by 6-Bev protons incident on the Be target were apparently not polarized, as the 320-Mev antiprotons scattered from Be and C were scattered equally left and right. The antiprotons were, in one experiment, selected from an angle of 7 deg in the Bevatron target and the left-right asymmetry of scattering in Be and C was less than 5%. It is reasonable to expect that the antiprotons would be polarized in the production process, and only a small fraction of those produced would be scattered in the internal target of the Bevatron. The small left-right asymmetry is thus surprising.



MU-19684

Fig. 15. Polarization of \bar{p} scattering from beryllium.

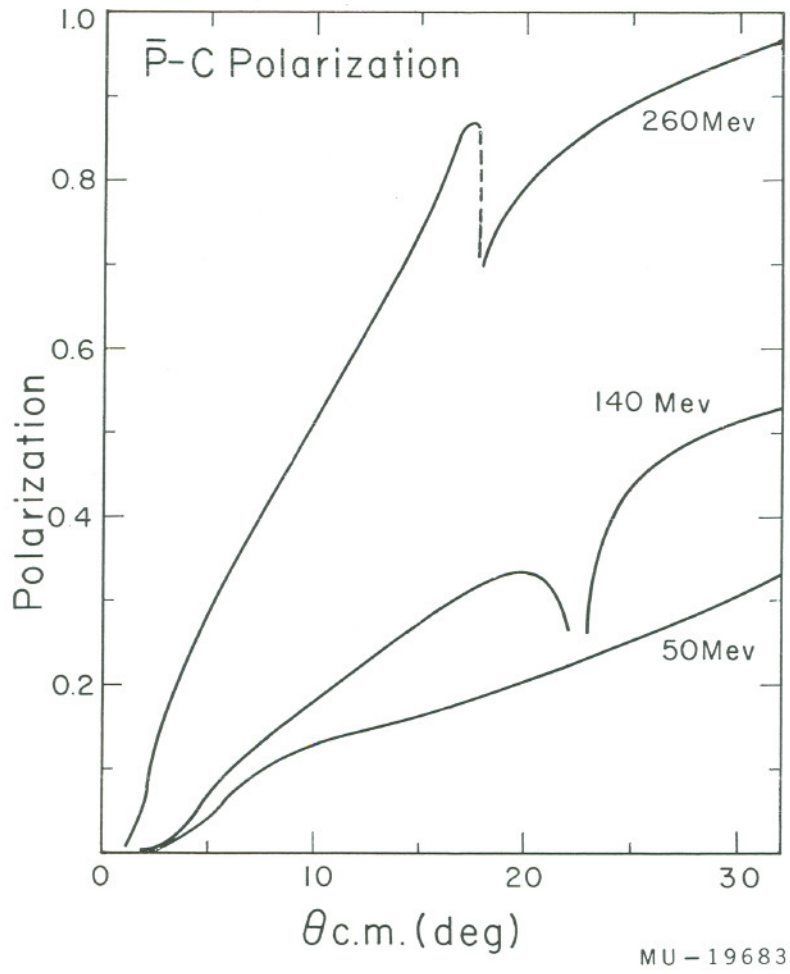


Fig. 16. Polarization of \bar{p} scattering from carbon.

IX. FERMI STATISTICAL MODEL

Fermi's statistical model²² can be used to predict the multiplicity of pions and K mesons produced by the annihilation process. For the capture process, the Fermi volume is

$$\Omega_0 = \frac{4\pi}{3} \left(\frac{\hbar}{m_\pi C^2} \right)^3$$

assuming statistical equilibrium, where m_π is the mass of the pion. The rest energy is $2 M_N C^2$, where M_N is the mass of a nucleon, using this simple model. The calculated annihilation volume is much too large to account for the large multiplicity of pions and the small number of K mesons. Koba and Takeda³ have devised a model to explain the observed results.²³ They have assumed that a nucleon is made up of a nucleon core and a pion cloud. Then, annihilation takes place only when the nucleon and antinucleon cores collide. Annihilation occurs in a time very short compared with the characteristic pion-cloud oscillation time. Thus, besides the pions that are produced by the annihilation of the cores, real mesons are shaken loose from the pion clouds. Estimates assuming this model give approximately 2.6 pions coming from the cloud and 2.2 from the cores, or a total of 4.8, in good agreement with the value 5.3 obtained by Barkas et al. from emulsions and the value of 5.0 obtained by Horwitz et al. from the hydrogen bubble chamber.²⁴

This model explains the small $K\text{-}\bar{K}$ production cross section too, because the K pair is expected to be produced in the core for the low-energy annihilation process. If the volume of the core is small, the volume in phase space is small for K-meson production.

X. CONCLUSIONS AND DISCUSSION

The technique using the 4π solid angle scintillation counter has been a very effective way of simultaneously measuring with one system of counters the elastic, inelastic, and charge-exchange cross sections and angular distributions. The experimental results of anti-proton-proton scattering are in very good agreement with the calculations of Ball and Chew (Figs. 6 and 7), and Ball and Fulco (Fig. 12). The annihilation and elastic cross sections of antiprotons are approximately equal over the energy range from 133 to 333 Mev (Table II). The charge-exchange cross section is approximately 10 mb over this energy range and agrees with calculations.

The observed scattering of antiprotons from Be and C is well described at small angles by use of the optical model. The experiments have not yet been done in sufficient detail at large angles to determine whether a first-diffraction minimum is present. However, this is a very feasible experiment. Calculations (Section VIII) have been made of the polarization of antiprotons scattered from Be and C. From the measured differential cross sections on Be and C of approximately 1000 mb/ster at 10 deg (c.m.) at 320 Mev, it appears quite feasible to do double-scattering experiments of antiprotons.

Experiments should be done at energies of 700 Mev and greater to determine the annihilation and elastic cross sections. These experiments will be more difficult because other inelastic processes can occur. For example, the threshold for production of pions is 290 Mev. Also, at 0.8 Bev, antihyperon-hyperon pairs should be made from antiprotons. This too is an interesting experiment.

The Ball-Chew model cannot be applied at high energies because of nucleon recoil effects, and penetration of the core by higher partial waves. This model predicts strong annihilation at low energies by having the pion cloud deflect the antinucleons inward so that they fall into the small black hole, the core. Thus, if these ideas are

valid, antiprotons in the Bev range will have too much momentum to be deflected by the pion cloud. Also, if the cross section is proportional to $(r + \kappa)^2$ then at high energies the annihilation cross section should decrease to the area of the black hole, or about 10 mb. If the multiple-meson-production events can be distinguished from the annihilation events, the character of the core can be determined.

The cross-section measurements at energies below 100 Mev are difficult with scintillation-counter techniques. However, by the use of several electromagnetic separators, a "clean" beam of low-energy antiprotons can be detected in a hydrogen bubble chamber. Besides the cross-section measurements, the multiplicity of pions and K mesons produced by annihilation can be determined. Dispersion relations can be tested by measuring the pion distribution from the annihilation process.³

ACKNOWLEDGMENTS

It is a very great pleasure to acknowledge the support, inspiration, and enthusiasm contributed by Professor Luis Alvarez. Discussions with Professor Geoffrey Chew, Professor Burton Moyer, Dr. William Wenzel, and Jose Fulco have been valuable in determining the aspects of current theories that could be most readily tested by experiment. The opportunity to work with my colleagues on the most recent antiproton experiments described here has been most rewarding. These collaborators included William Wenzel, Charles Coombes, Dr. William Galbraith, Glen Lambertson, and Dr. Oreste Piccioni.

Many of the new devices for the antiproton experiments have been developed with the generous support of personnel of the various shops.

The operation of the Bevatron has been under the direction of Dr. Edward J. Lofgren, with Walter Hartsough in charge of the operating crew.

This work was done under the auspices of the U. S. Atomic Energy Commission.

BIBLIOGRAPHY

1. J. S. Ball and G. E. Chew, Phys. Rev. 109, 1385 (1958).
2. J. R. Fulco, Phys. Rev. 110, 784 (L) (1958);
J. S. Ball and J. R. Fulco, Phys. Rev. 113, 647 (1959).
3. Z. Koba and G. Takeda, Progr. Theoret. Phys. (Kyoto) 19,
269 (1958).
4. Coombes, Cork, Galbraith, Lambertson, and Wenzel, Phys.
Rev. 112, 1303 (1958).
5. N. F. Mott and H. S. W. Massey, 2nd Edition 1949, Clarendon
Press, Oxford.
6. W. K. Panofsky and F. L. Fillmore, Phys. Rev. 79, 57 (1950);
Cork, Johnston, and Richman, Phys. Rev. 79, 71 (1950);
R. Christian and H. P. Noyes, Phys. Rev. 79, 81 (1950).
7. Selektor, Nikintin, Bogomolov, and Zombkovsky, Doklady
Akad. Nauk, SSSR 99, 967 (1954).
8. Cork, Wenzel, and Causey, Phys. Rev. 107, 859 (1957).
9. Wilmot N. Hess, Revs. Modern Phys. 30, 368 (1958).
10. H. P. Stapp, N. Metroplis, and T. J. Ypsilantis, Phys. Rev.
105, 302, (1957).
11. Landau and Smorodinsky, Lectures on Nuclear Theory (State
Technical-Theoretical Literature Press, Moscow, 1955).
12. S. Gartenhaus, Phys. Rev. 100, 900 (1955).
13. R. Christian and E. Hart, Phys. Rev. 77, 441 (1950).
14. P. Signell and R. Marshak, Phys. Rev. 106, 832 (L) (1957).
15. Fernbach, Serber, and Taylor, Phys. Rev. 75, 1352 (1949).
16. W. B. Riesenfeld and K. M. Watson, Phys. Rev. 102, 1157 (1956).
17. R. Serber and W. Rarita, Phys. Rev. 99, 629A (1953).
18. Cork, Lambertson, Piccioni, and Wenzel, Phys. Rev. 107,
248 (1957).
19. Chamberlain, Keller, Mermod, Segrè, Steiner, and Ypsilantis,
Phys. Rev. 108, 1553 (1957).
20. A. E. Glassgold Phys. Rev. 110, 220, (1958);
H. Duerr and E. Teller, Phys. Rev. 101, 494 (1956).

21. Frank E. Bjorklund and Sidney Fernbach, and Lewis E. Agnew, Jr. and Jose R. Fulco, (Lawrence Radiation Laboratory), private communications.
22. E. Fermi, *Progr. Theoret. Phys. (Kyoto)* 5, 570 (1950).
23. Barkas, Birge, Chupp, Ekspong, Goldhaber, Goldhaber, Heckman, Perkins, Sandweiss, Segrè, Smith, Stork, van Rossum, Baroni, Castagnoli, Franzinetti, and Manfredini, *Phys. Rev.* 105, 1037 (1957);
24. Horwitz, Miller, Murray, and Tripp, *Phys. Rev.* Vol. 115 No. 2 p. 472 1959.

This report was prepared as an account of Government sponsored work. Neither the United States, nor the Commission, nor any person acting on behalf of the Commission:

- A. Makes any warranty or representation, expressed or implied, with respect to the accuracy, completeness, or usefulness of the information contained in this report, or that the use of any information, apparatus, method, or process disclosed in this report may not infringe privately owned rights; or
- B. Assumes any liabilities with respect to the use of, or for damages resulting from the use of any information, apparatus, method, or process disclosed in this report.

As used in the above, "person acting on behalf of the Commission" includes any employee or contractor of the Commission, or employee of such contractor, to the extent that such employee or contractor of the Commission, or employee of such contractor prepares, disseminates, or provides access to, any information pursuant to his employment or contract with the Commission, or his employment with such contractor.